Hydra Observations of Aluminum Abundances in the Red Giants of the Globular Clusters M80 and NGC 6752

Robert M. Cavallo[1]

Lawrence Livermore National Laboratory, 7000 East Ave, L-97, Livermore, CA 94450

rcavallo@llnl.gov

Nicholas B. Suntzeff

Cerro Tololo Inter-American Observatory

National Optical Astronomy Observatory

Casilla 603, La Serena, Chile

and

Catherine A. Pilachowski

Astronomy Department, Indiana University, Swain West 319, 727 E. 3rd St, Bloomington, IN 47405

ABSTRACT

Aluminum and other metal abundances were determined in 21 red giants in the globular clusters NGC 6752 and M80 as part of a larger study to determine whether the aluminum distribution on the red giant branch is related to the second parameter effect that causes clusters of similar metallicity to display different horizontal branch morphologies. The observations were obtained of the Al I lines near 6700 Å with the CTIO Blanco 4-m telescope and Hydra multi-object spectrograph. The spectra have a resolving power of 18000 or 9400, with typical S/N ratios of 100-200. Mean [Fe/H] values obtained from the spectra are –1.58 for NGC 6752 and –1.73 for M80; this represents the first spectroscopic iron abundance determination for M80. Both NGC 6752 and M80 display a spread in aluminum abundance, with mean [Al/Fe] ratios of +0.51 and +0.37, respectively. No trend in the variation of the mean Al abundance with position on the giant branch is discernible in either cluster with our small sample.

Subject headings: globular clusters: individual (NGC 6752,M80) — stars: abundances — stars: horizontal branch — stars: late-type — stars: Population II

[1]Visiting Astronomer, Cerro Tololo Inter-American Observatory, National Optical Astronomy Observatory, which is operated by the Association of Universities for Research in Astronomy, Inc. (AURA) under cooperative agreement with the National Science Foundation.

1. INTRODUCTION

Over 20 years have passed since Norris et al. (1981) first showed aluminum abundance variations on the red-giant branch (RGB) of the globular cluster NGC 6752, and yet the nature of these inhomogeneities remains a mystery. Observations since then continue to show aluminum (and sodium and magnesium) variations in other clusters (see, e.g. Cottrell & Da Costa 1981; Wallerstein et al. 1987; Spite et al. 1987; Drake, Smith, & Suntzeff 1992; Norris & DaCosta 1995; Pilachowski et al. 1996; Zucker, Wallerstein, & Brown 1996; Shetrone 1996a; Kraft et al. 1997; Sneden et al. 1997; Kraft el al. 1998; Ivans et al. 1999; Cavallo & Nagar 2000; Ivans et al. 2001; Ramírez & Cohen 2001; Gratton et al. 2001; Grundahl et al. 2002). Although variations in carbon and nitrogen were previously known, these could be described through a simple mixing mechanism proposed by Sweigart & Mengel (1979), where rotationally induced meridional circulation currents could carry nuclearly processed materials such as C, N, and O from around the hydrogen-burning shell (H shell) of a red giant across the radiative zone to the outer convective envelope. Heavier elements such as Mg, Na, and Al weren't thought to be processed around the H shell, and any variations in them were taken as evidence that some kind of primordial pollution affected the surface abundances (see, e.g., Cottrell & Da Costa 1981). Continued work on key nuclear reaction rates (Champagne et al. 1988; Denisenkov & Denisenkova 1990; Iliadis et al. 1990; Champagne, Brown, & Sherr 1993; Blackmon et al. 1995; Iliadis et al. 1996), however, suggested that these elements could be processed around the H shell under the same conditions that the CN and ON nuclear cycles operated. Using these results, as well as the widely accepted rates of Caughlin & Fowler (1988), separate groups showed that it is possible to account qualitatively for the observed variations that showed Na, Al, and N anticorrelated with C, O, and, in some cases, Mg (Langer et al. 1993; Cavallo et al. 1996; Denissenkov & Weiss 1996; Cavallo et al. 1998; Denissenkov et al. 1998). The challenge has always been describing the results *quantitatively*; in particular, producing [Al/Fe] as high as 1.5 dex without overproducing [Na/Fe], and depleting ^{24}Mg to the observed levels in M13 (Shetrone 1996b), all while remaining within the acceptable proton-capture rates (Langer et al. 1997; Angulo et al. 1999; Powell et al. 1999; Iliadis et al. 2001). Despite any latitude afforded by the reaction rate uncertainties (see, e.g., Cavallo et al. 1998), the mixing theory still relies on non-solar abundance ratios in the star prior to mixing (Denissenkov et al. 1998; Cavallo & Nagar 2000), thus, at least partly relying on primordial influences. Theories other than meridional circulation have been put forth (Langer et al. 1997; Fujimoto et al. 1999; Aikawa, Fujimoto, & Kata 2001; Denissenkov & Weiss 2001), but a detailed discussion of each is beyond the intent of this paper.

Regardless of the physics behind any mixing mechanism, the question still remains: are the Al (and Na, Mg) variations caused by mixing, primordial sources, or a combination of both? We might be able to answer this question by looking at another long outstanding problem in globular cluster astronomy, namely, the second-parameter effect. First pointed out by Sandage & Wildey (1967) and van den Bergh (1967), the second-parameter effect refers to the phenomenon where the horizontal-branches (HB) of two clusters with similar metallicity (the first parameter) have markedly different color distributions. Possible second parameters that have been investigated

include age, initial helium abundance, CNO abundance, and mass loss (see, e.g., Faulkner 1966; Renzini 1977; Chaboyer et al. 1998), among others, but none is applicable to all clusters. One recent suggestion hypothesizes that if deep mixing (i.e., mixing that penetrates the H shell) occurs, then helium will be brought to the surface affecting the HB morphology by making mixed stars both bluer and brighter (Sweigart 1997a,b).

Unfortunately, helium cannot be measured in RGB stars because of their low surface temperatures, and helium settling on the HB precludes an accurate measurement in the hotter stars. However, models by Cavallo et al. (1998), which use standard (albeit, uncertain) reaction rates, show that aluminum can be produced only in the H shell of giants within the last magnitude of the RGB, implying that an increase in helium in the envelope must also be accompanied by an increase in aluminum. From this we can postulate that, if [Al/Fe] variations are produced internally and not primordially, Al could be a good surrogate to measure He mixing on the bright RGB, and if He mixing is indeed the second parameter, a relationship should exist between the ratio of Al-strong to Al-normal stars (the Al ratio) and the ratio of blue to red HB stars (the HB ratio). It is the *distribution* of abundances as a function of magnitude that is critical in determining the whether this correlation exists and what its cause might be.

This current work attempts to provide some fresh data on clusters that have been historically under-studied. Both M80 (NGC 6093) and NGC 6752 possess blue HBs relative to other clusters at similar metallicity. For example, Ferraro et al. (1998) compared Hubble U, V M80 photometry directly with M13 and M3, with the result that M80's HB is very similar to M13, while M3 lacked the extended blue tail of the other two clusters. Meanwhile, Grundahl et al. (1999) presented extensive Strömgren photometry of NGC 6752, M13, and M3, showing extensive blue tails in the former two compared with the latter. Neither M80 nor NGC 6752 had been studied extensively for abundances until Gratton et al. (2001) and Grundahl et al. (2002) determined [Al/Fe] for 39 stars in NGC 6752 in total, extending the data of Norris & DaCosta (1995). These were significant results because they probed less evolved stars near the main-sequence turnoff, on the subgiant branch, and at the base of the RGB, which are below the point that mixing theories predict that aluminum can be produced. Using a non-LTE analysis, Gratton et al. (2001) observed dwarfs with [Al/Fe] as low as -0.76 dex from the Al I resonance lines, and subgiants with [Al/Fe] as high as $+0.86$ dex from the doublet at $\lambda\lambda 8773/74$ Å. In fact, the resonance line analysis for the dwarfs yielded [Al/Fe] $= \ -0.18 \pm 0.15$ (s.e.m.) dex, while the subgiants gave [Al/Fe] $= \ +0.29 \pm 0.11$ dex (s.e.m.). The results for the dwarfs are uncertain due to the difficulty of analyzing resonance lines with non-LTE corrections of as much as +0.6 dex; yet, the results are still surprisingly low. What causes the drastic change from the main sequence to the subgiant branch: atmospheric effects, the different choice of lines, or an actual physical phenomenon? The Grundahl et al. (2002) results are more in line with the results of Norris & DaCosta (1995) and with other clusters. We discuss implications of the aluminum data in NGC 6752 in more detail in section 6.2.

M80, on the other hand, has no published abundances and is in need of further investigation, especially given its similarities to M13 in metallicity and HB morphology.

The rest of the paper is outlined according to the following: We begin with a description of the observations in Section 2, followed by our data reduction techniques in Section 3. We then discuss membership criteria in Section 4. After culling the data, we show the results of our abundance analysis in Section 5 and give our final conclusions in Section 6.

2. OBSERVATIONS

Between 1999 and 2001 we used the CTIO Blanco 4m telescope with the Hydra multi-object spectrograph in the echelle mode to observe 105 stars near NGC 6752 and 47 stars near M80. In the end, only a subset of these spectra were of sufficient quality to determine both cluster membership and abundance information. We describe the observations in the following two subsections, and discuss the radial velocity membership criteria in Section 4.

2.1. Observing Parameters and Instrument Configurations

Our observations were taken during two different epochs, between which the instrument underwent substantial changes. The first run was during the commissioning phase of Hydra in 1999, and only concentrated on NGC 6752 giants, while the second run occurred in 2001, and involved both clusters. The different instrument parameters for each epoch are listed in Table 1. The net effect of the change between the two runs is the higher resolution offered in 2001 by placing slit plates in front of the large fibers and using the longer focal-length camera. The resolution was measured using the FWHM of narrow emission lines in the comparison lamps. Both observing runs utilized the echelle grating.

2.2. Targets

Comprehensive membership surveys were available for neither M80 nor NGC 6752 when stars were selected for observation with Hydra, limiting our ability to ensure that fibers were assigned to actual cluster members and not to field stars. Both clusters are located at relatively low galactic latitude (+19 degrees for M80 and –25 degrees for NGC 6752), and field star contamination is likely without proper motion or radial velocity information. For NGC 6752, we used the B, V photographic photometry of Buonanno et al. (1986) to select likely cluster members. This cluster has a large tidal radius of $55.'34$ (Harris 1996), compared with the $40'$ field of view for Hydra, ensuring that most stars in the aperture were likely to be members.

Since no wide-field photometry exists for M80, we obtained B, V CCD photometry of nine $13' \times 13'$ fields centered on M80 with the CTIO 0.9m telescope prior to our Hydra run. The weather was not photometric, but we were able to obtain reasonable estimates of colors ($\pm$ $0.^{\rm m}05$), and

accurate astrometry after tying the system to the USNO-A2.0 catalog (Monet et al. 1998).

As a best guess for determining actual members of both clusters prior to our runs, we combined the existing photometry with the available proper motion data. For both clusters, we received accurate astrometric data from D. Dinescu (1998, 2001, private communication), which also included proper motion information. The average proper motions for 998 NGC 6752 stars in the Dinescu sample were $\mu_\alpha = -0.5 \pm 23.0$ (1σ) mas yr^{-1}, and $\mu_\delta = +3.0 \pm 31.0$ (1σ) mas yr^{-1}, around the cluster center. We selected for observation only stars with $-14.2 \leq \mu_\alpha \leq +13.7$ mas yr^{-1}, and $-9.8 \leq \mu_\delta \leq +9.9$ mas yr^{-1} for observing. Dinescu's data for M80 were for stars in an annulus far outside the small cluster, and were less useful for selecting probable members.

The final lists of stars that we ultimately determined to be cluster members and that had spectra with sufficient S/N to analyze reliably are given in Tables 2 and 3. The star identification in the first column in Table 2, as well as the photometry for the NGC 6752 giants are from Buonanno et al. (1986), while the alternate name in column 2 is from Dinescu's work. The colors for NGC 6752 are corrected assuming $E(B - V) = 0.04$, as listed by Buonanno et al. (1986). The exposure times and S/N near 6700 Å are listed for each observing run separately. For M80, the star number and photometry are our own[1], with $E(B - V) = 0.17$ magnitudes assumed (Kron & Guetter 1976; Reed, Hesser, & Shawl 1988). Despite the rather large list of stars that we observed, only 21 made it past the cutting room floor. The main obstacle to obtaining more spectra was the need for both high S/N and high resolution, which was aggravated by varying observing conditions and intermittent mechanical difficulties during the commissioning of Hydra.

3. CCD PROCESSING AND SPECTRA EXTRACTION

The data from both epochs were processed in similar fashion using the reduction routines in IRAF (Tody 1986), beginning with the usual overscan and bias corrections. We made our flat-field image by combining several daytime sky flats that were exposed by using diffusing filter in place of the echelle filter, removing the spectral shape in the x and y directions by curve-fitting, and boxcar filtering the remainder, which left us with a smooth milky flat that contained only pixel-to-pixel variations. The data images were then divided by this flat. The object spectra were extracted using the IRAF task APALL with variance weighting, background subtraction, and cosmic-ray cleaning parameters turned on. The fiber-to-fiber response functions were calculated using the MSRESP1D task, where the individual fiber responses in an averaged quartz flat were determined with reference to an averaged twilight sky flat. To remove fiber-to-fiber variations as well as most of the instrument profile, these responses were then divided through the extracted spectra to create normalized spectra.

To determine the dispersion solutions for both epochs, we used etalon exposures bracketed

[1]The astrometry is available from the first author.

around our object exposures throughout the night. These nighttime etalon spectra were calibrated with "master" etalon spectra that were acquired early during the first night of each run and were themselves calibrated from a ThAr lamp for the first epoch, and a HeNeAr lamp for the second epoch. The dispersion solution for a gas-filled lamp was applied to the extracted master etalon spectra, which were then averaged together to form one spectrum. The individual lines in the averaged master etalon spectrum were then measured and used to calibrate the individual spectra from the master etalon image so that every fiber used the same set of lines in its dispersion solution. These master etalon spectra were then used to calibrate the nighttime etalon spectra. We checked the quality of our etalon solutions by comparing ones taken on two different nights and found that both fiber-to-fiber and night-to-night dispersion solutions remained consistent to less than 0.002 Å.

We prefer using the etalon because of its superior precision. For example, during the second epoch the HeNeAr exposure only contained 17 usable lines over ∼300 Å, with most lines on the red side of the spectrum, while the etalon contained 95 strong unblended lines uniformly spaced over the spectrum. The typical rms for the HeNeAr lamp was around 0.03 Å while the etalons were better by an order of magnitude.

Sky spectra were obtained by pointing ∼20 of the available fibers at empty fields during the program star exposures. After extraction and calibration, the skies were averaged together to build a clean single background spectrum, which was subtracted from the object spectra. Finally, the program star spectra were flattened with a high order spline that was fitted through the continuum. No telluric line corrections were made since there were no telluric lines in our spectra during the second epoch and the ones appearing in the earlier data are outside our window of interest.

4. RADIAL VELOCITIES

After extracting and calibrating the spectra, we measured radial velocities in order to determine cluster membership. While the etalon lamps gave very high precision wavelength calibrations, they are uncertain in absolute wavelength. Raw radial velocities were determined for each star using strong lines in our highest S/N ratio spectra. We calibrated the velocity scale for each cluster observation by setting the mode of the velocity distribution equal to the published radial velocity, using $+8.2 \pm 1.5$ (1σ) km s^{-1} for M80 and -27.9 ± 0.8 (1σ) km s^{-1} for NGC 6752 (Harris 1996). We accepted for further study all stars that that had radial velocities within 22 and 15 km s^{-1} of the cluster means for M80 and NGC 6752, respectively, and which have sufficient S/N ratio for reliable abundance determinations (typically above 100 for epoch 1 and 60 for epoch 2).

5. ABUNDANCE ANALYSIS

5.1. Equivalent Widths

We determined a set of lines to measure by examining the spectra with the highest S/N from each set of cluster giants. The lines were identified and compared with the solar spectrum of Wallace, Hinkle, & Livingston (1993), and with Table II of Thévenin (1990), from which the oscillator strengths were chosen, with the following exceptions: the wavelengths and excitation potentials of the Fe I lines come from Nave et al. (1994), and we use the atomic data for the Eu II line at λ6645 Å that is consistent with hyperfine splitting, as described in sec 5.3. This produced an Eu oscillator strength that is +0.22 dex stronger than the value listed by Shetrone (1996a) and is +0.51 dex stronger than the Thévenin (1990) value. For the other lines, we used only those that Thévenin (1990) cites as having an uncertainty in log gf of less than 0.05 dex, and stayed away from strong blends where the separate cores of each line could not be individually detected in our spectra. We measured equivalent widths using Gaussian fits with the IRAF routine SPLOT and made use of the SPLOT deblending algorithm for lines that overlapped, but appeared visually distinct. The line list and equivalent widths are given in Table 4 for NGC 6752, and Table 5 for M80.

To check for consistency from epoch to epoch, we measured the equivalent widths of 12 lines in the spectra of seven NGC 6752 giants that were observed during both runs, and show the results in Figure 1, where the solid line represents perfect agreement. The average difference between the two datasets is 2.61 $\pm$ 8.89 mÅ (1 σ), in the sense of the 2001 data minus the 1999 data. Considering the different instrument capabilities between the two epochs and the different S/N quality of the datasets, we consider this to be good agreement.

5.2. Model Parameters: $T_{\rm eff}$, Gravity and Microturbulence

We explored two methods of determining model atmosphere parameters: spectroscopically from Fe I lines, and photometrically from B, V colors. Each method proved equally challenging, yet both provided consistent results.

To derive atmospheric models from Fe I lines, we employed the usual approach of removing dependencies of the derived abundances on both the excitation potentials and the reduced widths[2] to derive $T_{\rm eff}$ and $v_{\rm t}$, respectively. We used MOOG (Sneden 1973, , version 2000), the LTE analysis routine, in conjunction with MARCS (Gustafsson et al. 1975), the plane-parallel stellar atmosphere code, to determine all the abundances in this paper. The gravities were determined by interpolating between effective temperatures in a 12 Gyr isochrone with [Fe/H] $= -1.54$ and [α/Fe] $= +0.3$, provided to us by R. Bell [1999, private communication; see Houdashelt, Bell, & Sweigart (2000)].

[2]Reduced width = equivalent width divided by wavelength.

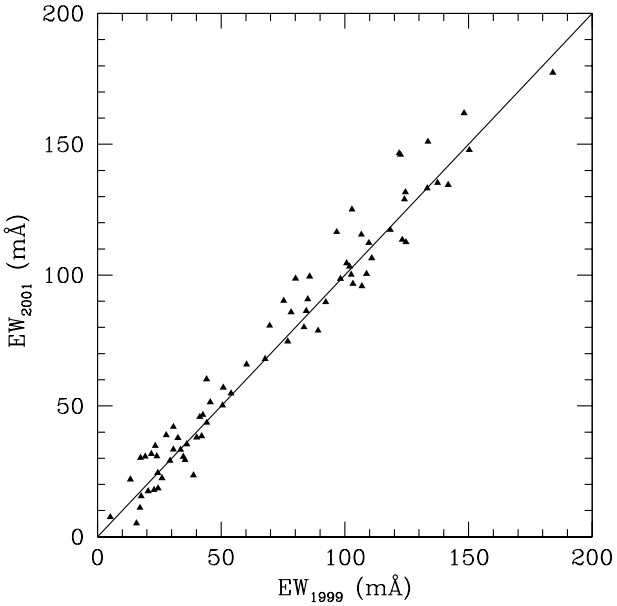

Fig. 1.— Comparison of equivalent widths from a sample of spectra observed in both 1999 and 2001. The diagonal line represents perfect agreement.

The difficulty with this approach is two-fold: first there are only a handful of Fe I lines available in the spectra, and usually only enough in the brightest (and coolest) stars to determine parameters. Second, recent work has revealed possible problems with determining [Fe/H] using Fe I lines due to NLTE effects (Thévenin & Idiart 1999), which are most exaggerated at lower metallicities and for low excitation-potential lines. The Thévenin & Idiart (1999) results, however, are from main-sequence turn-off stars and it appears from their work and from Kraft & Ivans (2003) that the "overionization" problem that might cause difficulties in less evolved stars probably isn't a concern here.

We also derived $T_{\rm eff}$ photometrically with the color-corrected B, V data from Buonanno et al. (1986) for NGC 6752, using the Bell isochrone discussed above, which provides transformed colors in B and V. From this $T_{\rm eff}$ we determined an appropriate log g from the isochrone, and then found $v_{\rm t}$ via the empirical formula given by Pilachowski et al. (1996); i.e., $v_{\rm t} = -8.6{\times}10^{-4}T_{\rm eff} + 5.6$ km s^{-1}. This approach provides microturbulent velocities that are, on a star-by-star basis, systematically higher by $0.24 \pm 0.161\sigma$ km s^{-1} than those determined via Fe I lines. As discussed below, this has little effect on the final results. Comparing $T_{\rm eff}$ from the spectroscopy with $T_{\rm eff}$ from the photometry for 11 NGC 6752 giants that had spectra with S/N $>$ 65 and at least 11 Fe I lines over a range of excitation potential from 1.0 eV to 4.8 eV, we found an average difference of -39 ± 81 (1σ) K, with the spectroscopic determination yielding the lower values on average. Removing the most discrepant case, star 277, reduces $T_{\rm eff-spectrum} - T_{\rm eff-photometry}$ to -17 ± 48 (1σ) K. The agreement is quite good given the uncertainties in the photometry and small number of Fe I lines, indicating that

either approach is sufficient for determining model atmosphere parameters. A similar analysis for the M80 giants shows the spectroscopic temperatures to be 5 ± 65 (1σ) K lower on average than the photometric determinations.

The brightest giant studied in NGC 6752, star 3589 in the Buonanno photometry, also has a color that is both too red for our isochrone at its magnitude, and inconsistent with the next brightest giant, star 2403, which is only 0.1 magnitudes below it on the RGB; however, $T_{\rm eff}$ determined from the spectrum of star 3589 is only 25 K cooler than star 2403, indicating that its color is either in error, and it most likely belongs on the bright RGB, or that it is a variable star.

The model atmosphere parameters for our giants are listed in Table 6 for both clusters, with the method chosen for deriving the parameters indicated in column 5. Where possible, we used the photometrically derived parameters, but occasionally had to rely on the spectroscopic models when the photometry appeared questionable. This preference allowed us to utilize spectra that had lower S/N ratios than would be required to derive $T_{\rm eff}$ and $v_{\rm t}$ spectroscopically. Because of the lower resolution of the first epoch data, we still, nonetheless, needed high S/N ($\gtrsim$ 110) to derive abundances, while a factor of two lower S/N was sufficient for the second-epoch data.

Finally, we examine the sensitivity of our abundances on our choice of model atmosphere parameters, as shown in Table 7. The top row shows a reasonable estimate for the uncertainties in $T_{\rm eff}$, while giving even wider latitude in $\Delta\log\, g$ and $\Delta v_{\rm t}$. The variations are determined using the model and data from star 2240 in NGC 6752, which has a $T_{\rm eff}$ that is near the median value for our sample. Since the sensitivity to the parameters is not symmetric, we report in the table the worse result of either increasing or decreasing a given parameter. Only the 2001 data are used in this test since the spectrum has both a full complement of lines and a high S/N. The results are not surprising: $T_{\rm eff}$ plays the biggest role in the error budget, with the low E. P. lines of Ti I and Cr I being the most sensitive, while the ionized lines are little affected. Except for Ti II and Eu II, an increase in $T_{\rm eff}$ leads to an increase in [abundance/H]. Uncertainties in log g lead to only small errors for even the pressure-sensitive ions with some elements increasing with log g (Al, Ca, Ti I, and Cr) and others decreasing (Ti II, Fe, Ni, La, and Eu). Finally, uncertainties due to $v_{\rm t}$ are quite small, which is consistent with the many weak lines employed in our analysis. Increasing $v_{\rm t}$ desaturates the line thereby increasing the derived abundance, which is what we find in our results, with [Al/Fe] having zero dependence within the $v_{\rm t}$ uncertainties. Of course, the three parameters are not uncorrelated, so variations in one necessarily lead to variations in the others (as can be seen by the formula for $v_{\rm t}$, which is a function of $T_{\rm eff}$) and the sensitivities reported in Table 7 can be be modified to reflect this in the total uncertainty due to the atmospheric models. Since the focus of this study is primarily on aluminum, we note that the model uncertainties introduce only ~ 0.1 dex uncertainty in the [Al/Fe] ratio.

5.3. Results

In Table 8 we present the abundances of 11 stars in NGC 6752 and 10 in M80. These were accepted as cluster members after determining that their derived [Fe/H] ratios were consistent with the anticipated metallicities of each cluster, around -1.5 to -1.6 dex. We estimate that the abundances are uncertain by about 0.15 dex after accounting for line-to-line scatter, uncertainties in oscillator strengths and atmospheric parameters, and instrumental errors. The abundances for the NGC 6752 data are averaged together when available by giving the second-epoch results twice the weight of the first to account for the factor of two improvement in resolution. With the exception of star 3589, the abundances for NGC 6752 from the the two epochs were determined with a single model for each star as given in Table 6. For star 3589, we used the separately derived models given in Table 6 to derive abundances for each epoch before forming the weighted average. Of course, M80 was observed during only the second epoch and the results were derived with the models listed in Table 6. The iron abundances assume a solar value of $\log \epsilon = 7.52$, and the rest of the abundances are on the Anders & Grevesse (1989) scale. The aluminum and lanthanum abundances are not corrected for hyperfine splitting (hfs), but the europium data are. The hfs line list for the λ6645 Å line was provided to us by C. Sneden (2002, private communication) and we used the blends driver in MOOG to determine the abundances. The aluminum abundances are derived from only λ6696 Å, since this feature is stronger than the other half of the doublet, and is often visible even when λ6698 Å is not. Most [Al/Fe] values were determined from equivalent width data, except for NGC 6752 – 3011 and M80 – 5, for which we fit synthetic spectra as required by the very weak lines. All other abundances were determined via the equivalent width force-fitting routine in MOOG.

For lines that are indistinguishable from noise, we include estimates for upper limits to [Al/Fe] for several stars in Table 8. These limits are found by fitting a synthetic spectrum to the data, then adding noise to the synthetic fit with an iterative Monte Carlo routine that outputs a noisy spectrum with a S/N ratio that is consistent with the actual data. We iterate until the S/N ratio of the noisy synthetitc spectrum is within 5% of the S/N of the data. The synthetic spectrum is also sampled with the same spacing as the data and the line width is set by fitting a Gaussian to the Al I line at λ6696 in a spectrum where it is easily measured. The output is then compared by eye to the actual data. This approach alleviates the challenge of trying to decide when a fit of a perfect synthetic spectrum to a real, noisy spectrum is actually measuring data or measuring noise. All syntheses were carried out for the 2001 data, which had both high signal and superior resolution. In Figure 2, we show an example of the output from our routine for star NGC 6752 – 2403. The S/N ratio of the data in this region is 124, versus 120 in the "noisy" synthesis. The results appear to indicate that the data might be a marginal detection of a weak Al I feature at λ6696; however, we choose to err on the side of caution and consider this an upper limit.

The motive for deriving upper limits is to determine whether or not these stars might still be Al rich or whether they actually are Al normal and the Al lines are undetectable because of temperature, S/N ratio, or resolution. The three stars in Table 8 with upper limits are indeed

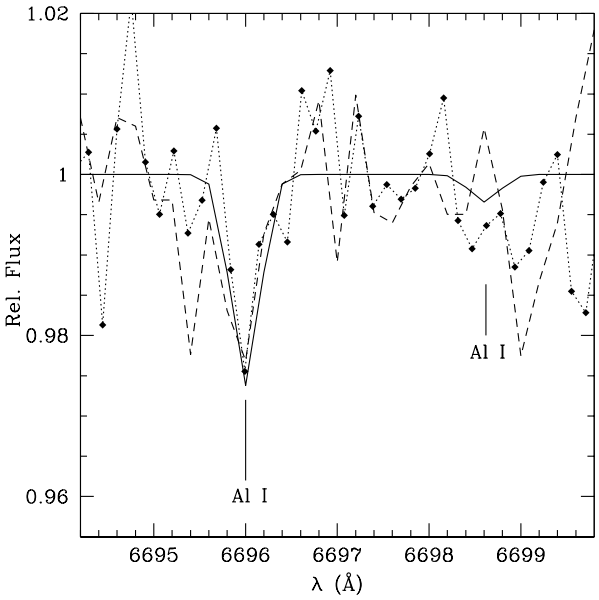

Fig. 2.— Example of output from a Monte Carlo routine that adds noise (dashed line) to a synthetic spectrum (heavy solid line). The data are shown by filled diamonds connected by a light dotted line.

Al-normal to Al-poor.

5.4. Discussion

5.4.1. Aluminum

The intent of this research is to discover the nature of the [Al/Fe] distribution in these two clusters, and we can make some observations despite the limited sample size. Figure 3, which shows [Al/Fe] as a function of the $T_{\rm eff}$, demonstrates that there is a broad distribution along the RGB with no discernible trends in the Al ratio for either cluster. As shown in Table 9, which summarizes the mean abundances by cluster, aluminum is enhanced in both clusters and shows the largest distribution among the elements studied, suggesting that the abundance spread is not statistical. That the variations are real is further supported in Figure 4, which shows the spectra of two stars with very similar atmospheric parameters from each cluster having largely varying Al I lines. Our results are consistent with the giants studied by Norris & DaCosta (1995) and Grundahl et al. (2002), and with the subgiants of Gratton et al. (2001). It would be useful to know how this distribution changes with magnitude by using the data of Gratton et al. (2001) and Grundahl et al. (2002), but theirs were purposely chosen in a biased manner according to c_1 indices and are understandably incomplete, given the large number of stars in the magnitude ranges where they

were operating, so that the data are insufficient to reveal any evolution of the Al ratio. If our results are representative of the clusters' [Al/Fe] distributions in general, then one would have to rule out the connection between the Al ratio and the HB morphology, since we expect any ongoing mixing to create an upward trend in [Al/Fe] with decreasing $T_{\rm eff}$, which is not seen here for this small sample. Whether these [Al/Fe] distributions truly represent the actual distributions in these clusters needs to be demonstrated with larger datasets.

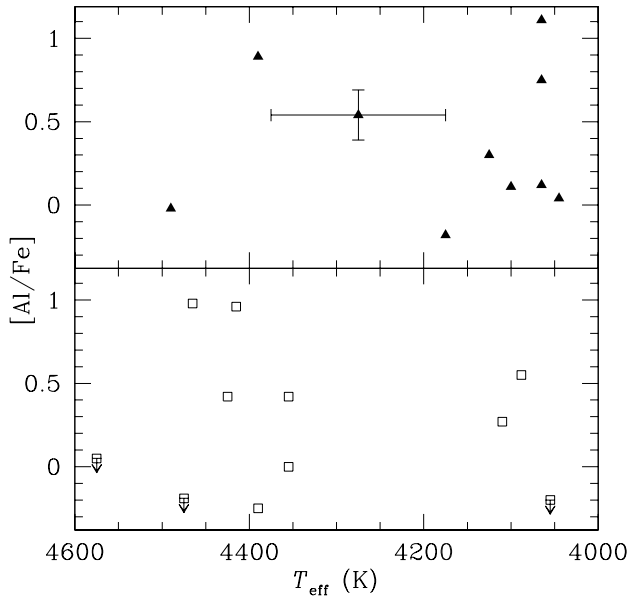

Fig. 3.— [Al/Fe] as a function of $T_{\rm eff}$ for both clusters. M80 data are denoted by filled triangles in the top panel and NGC 6752 data by empty squares in bottom panel. The upper limits for the NGC 6752 data from Table 8 are shown as empty squares with downward pointing arrows. The error bars shown in the top panel are representative of all the data presented.

5.4.2. Other elements

We look briefly at the other elements that had lines present in our spectra. Consistent with other clusters, calcium, an α-element, is enhanced by $\sim$0.25 dex relative to solar for both clusters. On the other hand, titanium is difficult to interpret; the neutral lines do not always agree well with the results from the ionized lines. On average the $[{\rm Ti/Fe}]_{\rm II}$ abundances are higher than the neutral-line abundances, possibly indicating miscalculated gravities, NLTE effects, poor oscillator strengths, or a combination of any of these. With regard to the gravities, we show in Table 7 that even a 0.2 dex change in log g results in less than a 0.1 dex change in [Ti/Fe] as determined from the Ti II lines, indicating that the discrepancy from the various lines probably has some other source. The Fe-peak elements chromium and nickel track iron with no unusual trends.

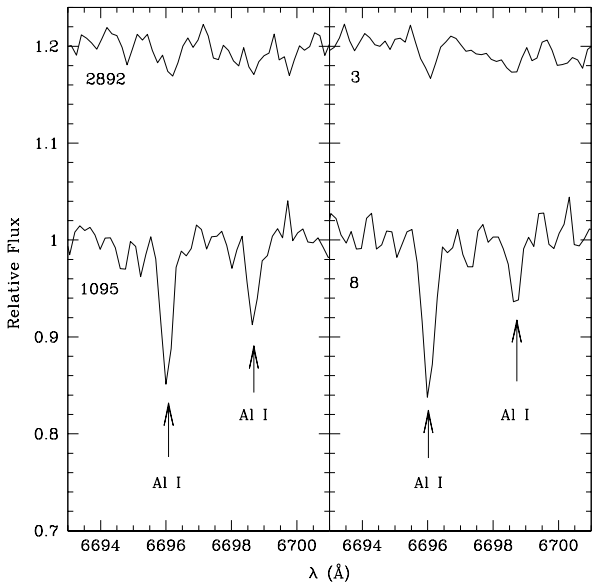

Fig. 4.— Two spectra each from NGC 6752 (left panel) and M80 (right panel) that show strong variations in their Al I features. The spectra for each cluster are taken from stars with similar effective temperatures. The fluxes have been shifted for clarity.

In both clusters the abundance of the neutron-capture element Eu is significantly enhanced relative to Fe, particularly for M80, while [La/Fe] is somewhat less enhanced for M80, and not at all for NGC 6752; however, the ratio of [Eu/La] remains constant at +0.42. This number is consistent with the results of Ivans et al. (2001) for M5, where the mean [Eu/La] is +0.40. We do note that a straightforward comparison of lanthanum and europium abundances with the work of other authors is inhibited by the fact that different authors use different atomic data, particularly when correcting for hfs effects, where the data are scarce and change frequently. Still, the mean [Eu/Fe] for M80 is higher than seen in M13, which has $< [\mathrm{Eu/Fe}] > \; = \; +0.44 \pm 0.11$ (1σ) (Shetrone 1996a), or in either NGC 288 or NGC 362, which are enhanced by ∼0.55 dex (Shetrone & Keane 2000). In both papers the authors use a log gf of +0.20, which if put on our scale would cause their abundances to decrease by 0.22 dex, making the discrepancy even larger.

Finally, we note via the λ6707 Å Li I feature that no cluster stars showed evidence for having enhanced lithium, as observed by Kraft et al. (1999) in M3, and is consistent with the results of Pilachowski et al. (2000).

6. CONCLUSIONS

6.1. Summary

We begin the conclusions by summarizing our results:

- We observed 21 giants in the globular clusters M80 and NGC 6752 with spectra of sufficient quality to determine abundances.
- Both M80 and NGC 6752 display a spread of aluminum abundances, having mean abundances of +0.37 dex and +0.51 dex, respectively. The abundance spreads are 0.43 (1σ) dex for M80 and 0.36 (1σ) dex for NGC 6752.
- The aluminum data cannot resolve the discrepancy in the [Al/Fe] values near the main-sequence turnoff and the subgiants as observed by Gratton et al. (2001).
- No trends between [Al/Fe] ratios and magnitude are discernible in our small sample.
- The mean [Fe/H] value for M80 is −1.73, which is the first spectroscopic determination for this cluster. For NGC 6752, the mean [Fe/H] is −1.58, which is consistent with previous results.
- The Fe-peak elements chromium and nickel follow iron closely.
- The [Ca/Fe] enhancements are consistent with the α-enhancements observed in other clusters.
- The [Eu/La] ratio is constant for both clusters at +0.42 dex, which does not appear unusual; however, both [Eu/Fe] and [La/Fe] are enhanced in M80 relative to NGC 6752.

6.2. A Final Look At Aluminum

Now that we've derived aluminum abundances in M80 and NGC 6752, are we any closer to answering whether or not the variations are the result of primordial pollution, mixing processes, or both? Perhaps when combined with the results of Grundahl et al. (2002) we can get some insight into just how complicated this problem really is (we do not include the Gratton data here since they were biased by use of the c_1 index to select stars.) Given the differences in the quality of the data between the two studies, and the still small number of stars that have been analyzed, it is difficult to draw firm conclusions. If mixing is an ongoing phenomenon, then one would expect that the Al ratio would increase with decreasing magnitude, as it appears to in M13 (Cavallo & Nagar 2000); unfortunately, the small numbers make this difficult to discern at this point.

An interesting result also comes from both Gratton et al. (2001) and Grundahl et al. (2002), who show that stars on the subgiant/lower red giant branch may have just as much Al in them as stars on the upper RGB, where mixing is theoretically possible. These results might suggest

that all Al anomalies are the result of pollution, but this raises yet another question: Can it be demonstrated that a globular cluster main sequence star, subgiant, or lower red giant exists that has strongly enhanced Al and is not depleted in C and/or O? That is, if the CNO variations are the result of deep mixing and the Al (and Na) anomalies are primordial, there should be stars that show uncorrelated abundance patterns. But, if the CNO and Na-Al anomalies are both caused by primordial scenarios, then why does evidence exist, in clusters where it's been studied, that the total C+N+O remains constant from star to star independent of the Na or Al content (Suntzeff 1981; Pilachowski 1988; Dickens et al. 1991), and how does one explain $^{12/13}$C ratios near the CN cycle equilibrium value in many other clusters (Suntzeff & Smith 1991; Shetrone 1996b; Zucker, Wallerstein, & Brown 1996; Briley et al. 1997a,b)? On the other hand, if the anomalies are all created *in-situ*, what is the physics behind them that can occur without completely contradicting well-established basic theories of stellar evolution? It used to be that one could side with one scenario or the other, then the data became more complicated, and one would say that it was somehow a mixture of both primordial and evolutionary scenarios. Maybe in the end that will be the final conclusion, but we are far from proving it; too many questions remain to be answered and too many observations remain to be made.

We thank D. Dinescu for providing us with valuable proper motion data, P. Palunas for aiding us with coordinate system transformations, and S. Keller for helping us with our photometry. We also wish to thank C. Sneden for providing us with both useful atomic data and advice on running MOOG. Finally, we thank our anonymous referee for his/her careful reading of our manuscript and helpful comments. In addition, R. M. C. acknowledges the National Research Council for support during a part of this work, as well as the AAS Small Research Grant program, and the Djehuty Stellar Evolution Project. This work was performed under the auspices of the U.S. Department of Energy, National Nuclear Security Administration by the University of California, Lawrence Livermore National Laboratory under contract No. W-7405-Eng-48. C.A.P. gratefully acknowledges support from the Daniel Kirkwood Research Fund at Indiana University. This research has made use of the SIMBAD database, operated at CDS, Strasbourg, France.

REFERENCES

Aikawa, M., Fujimoto, M. Y., & Kato, K. 2001, ApJ, 560, 937

Anders, E. & Grevesse, N. 1989, Geochim. Cosmochim. Acta, 53, 197

Angulo, C. et al. 1999, Nucl. Phys. A, A656, 3

Blackmon, J. C., Champagne, A. E., Hofstee, M. A., Smith, M. S., Downing, R. G., & Lamaze, G. P. 1995, Phys. Rev. Lett., 74, 2642

Briley, M. M., Smith, V. V., King, J., & Lambert, D. L. 1997a, AJ, 113, 306

Briley, M. M., Suntzeff, N. B., Smith, V. V., Bell, R. A., & Norris, J. 1997b, BAAS, 189, 1363

Buonanno, R., Caloi, V., Castellani, V., Corsi, C., Fusi Pecci, F., & Gratton, R. 1986, A&AS, 66, 79

Caughlin, G. R. & Fowler, W. A. 1988, Atomic Data and Nuclear Data Tables, 40, 283

Cavallo, R. M., & Nagar, N. M. 2000, AJ, 120, 1364

Cavallo, R. M., Sweigart, A. V., & Bell, R. A. 1996, ApJ, 464, L79

Cavallo, R. M., Sweigart, A. V., & Bell, R. A. 1998, ApJ, 492, 575

Chaboyer, B., Demarque, P., Kernan, P. J. and Krauss, L. M. 1998, ApJ, 494, 96

Champagne, A. E., Brown, B. A., & Sherr, R. 1993, Nucl. Phys. A, 556, 123

Champagne, A. E., et al. 1988, Nucl. Phys. A, 487, 433

Cottrell, P. L., & Da Costa, G. S. 1981, ApJ, 245, L79

Denissenkov, P. A., Da Costa, G. S., Norris, J. E. & Weiss, A. 1998, A&A, 333, 926

Denisenkov, P. A., & Denisenkova, S. N. 1990, Sov. Astron. Lett., 16, 275

Denissenkov, P. A., & Weiss, A. ApJ, 559, L115

Denissenkov, P. A., Weiss, A. & Wagenhuber, J. 1997, A&A, 320, 115

Denissenkov, P. A. & Weiss, A. 1996, A&A, 308, 773

Dickens, R. J., Croke, B. F. W., Cannon, R. D., & Bell, R. A. 1991, Nature, 351, 212

Drake, J.J., Smith, V. V., & Suntzeff, N., B. 1992, ApJ, 395, L98

Faulkner, J. 1966, ApJ, 144, 978

Ferraro, F. R., Paltrinieri, B., Fusi-Pecci, F., Rood, R. T., & Dorman, B. 1998, ApJ, 500, 311

Fujimoto, M. Y., Aikawa, M., & Kato, K. 1999, ApJ, 519, 733

Gratton, R. G., et al. 2001, A&A, 369, 87

Grundahl, F., Briley, M., Nissen, P. E., & Feltzing, S. 2002, A&A, 385, L14

Grundahl, F., Catelan, M., Landsman, W. B., Stetson, P. B., & Anderson, M. I. 1999, ApJ, 524, 242

Gustafsson, B., Bell, R. A., Eriksson, K., & Nordlund, Å. 1975, A&A, 42, 407

Harris, W. E. 1996, AJ, 112, 1487

Houdashelt, M. L., Bell, R. A., & Sweigart, A. V. 2000, AJ, 119, 1448

Iliadis, C., et al. 1990, Nucl. Phys. A, 512, 509

Iliadis, C., Buchmann, L., Endt, P. M., Herndel, H., & Weischer, M. 1996, Phys. Rev. C, 53, 475

Iliadis, C., D'Auria, J. M., Starrfield, S., Thompson, W. J., & Wiescher, M. 2001, ApJS, 134, 151

Ivans, I. I., Kraft, R. P, Sneden, C, Smith, G. H., Rich, R. M., & Shetrone, M 2001, AJ, 122, 1438

Ivans, I. I., Sneden, C., Kraft, R. P., Suntzeff, N. B., Smith, V. V., Langer, G. E., & Fulbright, J. P. 1999, AJ, 118, 1273

Kraft, R. P. & Ivans, I. I. 2003, PASP, 115, 143

Kraft, R. P., Peterson, R. C., Guhathakutra, P., Sneden, C., Fulbright, J. P., & Langer, E. G. 1999, ApJ, 518, 53

Kraft, R. P., Sneden, C., Smith, G. H., Shetrone, M. D., & Fulbright, J. P. 1998, AJ, 115, 1500

Kraft, R. P., Sneden, C., Smith, G. H., Shetrone, M. D., Langer, G. E. & Pilachowski, C. A. 1997, AJ, 113, 279

Kron, G. E., & Guetter, H. H 1976, AJ, 81, 817

Langer, G. E., Hoffman, R., & Sneden, C. 1993, PASP, 105, 301

Langer, G. E., Hoffman, R. D., & Zaidins, C. S. 1997, PASP, 109, 244

Monet, D., et al. 1998, The USNO-A2.0 Catalogue, (U.S. Naval Observatory, Washington DC)

Nave, G., Johansson, S., Learner, R. C. M., Thorne, A. P., & Brault, J. W. 1994, ApJS, 94, 221

Norris, J., Cottrell, P. L., Freeman, K. C., & Da Costa, G. S. 1981, ApJ, 244, 205

Norris, J. E., & Da Costa, G. S. 1995, ApJ, 447, 680

Pilachowski, C. A. 1988, ApJ, 326, L57

Pilachowski, C. A., Sneden, C., Kraft, R. P., Harmer, D., & Wilmarth, D. 2000, AJ, 119, 2895

Pilachowski, C. A., Sneden, C., Kraft, R. P., & Langer, G. E. 1996, AJ, 112, 545

Powell, D. C., Iliadis, C., Champagne, A. E., Grossman, C. A., Hale, S. E., Hansper, V. Y., & McLean, L. K. 1999, Nucl. Phys. A, 660, 349

Renzini, A. 1977, Saas-Fee Advanced Course 7: Advanced Stages in Stellar Evolution, eds. P. Bouvier and A. Maeder (Sauverny, Switzerland: Observatoire de Genève), 151

Ramírez, S. V, & Cohen, J. G. 2001, AJ, 123, 3277

Reed, B. C., Hesser, J. E., & Shawl, S. J. 1988, PASP, 100, 545

Sandage, A., & Wildey, R. 1967, ApJ, 150, 469

Shetrone, M. D. 1996a, AJ, 112, 1517

Shetrone, M. D. 1996b, AJ, 112, 2639

Shetrone, M. D. & Keane, M. J. 2000, AJ119, 840

Sneden, C. 1973, ApJ, 184, 839

Sneden, C., Kraft, R. P., Shetrone, M. D., Smith, G. H., Langer, G. E, & Prosser, C. F. 1997, AJ, 114, 1964

Spite, M., Huille, S., Francois, P., & Spite, F. 1987, A&AS, 71, 591

Suntzeff, N. B, 1981, ApJS, 47, 1

Suntzeff, N. B., & Smith, V. V. 1991, ApJ, 381, 160

Sweigart, A. V. 1997a, ApJ, 474, L23

Sweigart, A. V. 1997b, in The Third Conference on Faint Blue Stars, eds. A. G. D. Philips, J. W. Liebert and R. A. Saffer (L. Davis: Schenectady), p. 3

Sweigart, A. V., & Mengel, J. G. 1979, ApJ, 229, 624

Thévenin, F. 1990, A&AS, 82, 179

Thévenin, F., & Idiart, T. P. 1999, ApJ, 521, 753

Tody, D. 1986, "The IRAF Data Reduction and Analysis System" in Proc. SPIE Instrumentation in Astronomy VI, ed. D.L. Crawford, 627, 733

van den Bergh, S. 1967, AJ, 72, 70

Wallace, L., Hinkle, K., & Livingston, W. 1993, N. S. O. Technical Report #93-001

Wallerstein, G., Leep, E. M., & Oke, J. B. 1987, AJ, 93, 1137

Zucker, D., Wallerstein, G., & Brown,

Table 1. Observing Conditions and Instrument Parameters

	Epoch 1	Epoch 2
Cluster(s)	NGC 6752	NGC 6752, M80
Dates (UT)	26 June 1999	22-23 June 2001
Fibers	Large[a]	Large[a]
Slit Plates (μ)	None	200[b]
$f_{\rm cam.}$ (mm)	229	400
CCD	Loral 1k×3k	SiTe 2k×4k
Binning	1×1	1×2
Central Wavelength (Å)	6725	6667
Resolution	9400	18000
$\Delta\lambda$[c] (Å)	485	300
Seeing ($''$)	1.4	0.74
Moon Age (days from new)	13	1-2

[a]300 μ ($2''$) fibers

[b]Projects to $1''.3$

[c]Refers to the width of the spectrum on the CCD

Table 2. Stars Observed in NGC 6752

Star (1)	Alt. (2)	V (1)	$(B-V)_0$ (1)	t_{exp} (s) (Epoch 1)	S/N (Epoch 1)	t_{exp} (s) (Epoch 2)	S/N (Epoch 2)
3589	231	10.85	1.73	9600	230	7200	130
2403	242	10.95	1.43	9600	190	7200	125
2113	244	11.23	1.37	9600	190	7200	135
277	379	11.43	1.13	9600	185	7200	135
2240	590	11.63	1.13	9600	275	7200	120
1518	250	11.82	1.07	16800	245	7200	75
3011	239	11.98	1.10	9600	135	7200	70
3805	136	12.00	1.08	9600	135	7200	95
1095	598	12.18	1.04	9600	130	7200	70
2892	268	12.22	1.03	16800	140	7200	90
4437	93	12.78	0.96	16800	100	7200	70

Note. — V and $B-V$ are from Buonanno et al. (1986), using their value of $E(B-V) = 0.04$ to correct the colors. Epochs 1 and 2 are described in Table 1.

References. — 1 (Buonanno et al. 1986), 2 (D. Dinescu 1998, private communication

Table 3. Stars Observed in M80

Star	V	$(B-V)_0$	t_{exp} (s)	S/N
1	12.83	1.44	13800	185
2	12.96	1.60	13800	120
3	12.97	1.42	13800	200
4	12.98	1.38	13800	130
5	12.99	1.30	13800	70
8	13.28	1.42	13800	60
11	13.40	1.20	13800	100
16	13.45	1.42	13800	90
23	13.72	1.02	13800	100
31	13.99	1.10	13800	110

Table 4. Atomic Line Parameters and Equivalent Widths for NGC 6752 Giants

λ (Å)	Species	E.P. (eV)	Log gf	3589	2403	2113	277	2240	1518	3011	3805	1095	2892	4437
6696.023	Al I	3.14	−1.35	57.5	···	28.7	23.8	13.0	35.9	6.5	67.9	59.0	···	···
				55.3	···	···	25.6	17.4	25.9	···	54.4	56.5	···	···
6698.673	Al I	3.14	−1.65	30.8	···	12.3	···	···	···	···	28.7	23.3	···	···
				33.2	···	···	···	···	···	···	26.8	31.5	···	···
6717.687	Ca I	2.71	−0.39	···	···	···	···	···	···	···	···	···	···	···
				133.1	107.1	127.3	76.7	109.2	93.8	84.3	88.9	93.8	93.0	72.2
6599.113	Ti I	0.90	−2.06	118.0	22.1	57.6	16.4	32.2	12.2	···	···	···	···	···
				94.6	27.4	63.6	18.4	37.6	···	···	13.6	···	20.5	···
6743.127	Ti I	0.90	−1.76	126.9	42.4	74.5	···	51.4	33.4	27.7	···	···	17.9	···
				112.1	···	89.2	31.1	56.9	32.8	36.3	37.2	19.5	···	···
6606.979	Ti II	2.06	−2.85	···	···	27.2	···	19.7	···	···	··· 6	···	···	···
				27.4	21.9	35.6	17.8	19.9	···	···	21.6	···	···	···
6630.032	Cr I	1.03	−3.59	39.0	···	22.9	···	···	···	···	···	···	···	···
				44.1	···	···	···	11.9	···	···	···	···	···	···
6581.210	Fe I	1.49	−4.82	···	···	···	···	···	···	···	···	···	···	···
				89.0	55.2	70.2	30.9	···	47.9	···	40.6	38.3	34.5	···
6593.870	Fe I	2.43	−2.34	150.3	125.4	137.3	108.5	108.1	82.7	106.1	107.6	93.3	97.8	···
				147.8	129.0	151.0	115.5	106.5	116.5	95.8	96.7	89.7	98.6	80.1
6608.026	Fe I	2.28	−4.02	50.3	···	40.7	···	24.6	···	···	···	···	···	···
				52.4	27.2	43.9	15.3	25.4	20.6	20.0	···	20.2	···	10.4
6609.110	Fe I	2.56	−2.67	···	···	···	···	···	···	···	···	···	···	···
				116.4	85.1	106.1	81.3	85.7	84.7	62.6	74.9	65.3	66.0	58.2
6609.679	Fe I	0.99	−5.87	···	···	···	···	···	···	···	···	···	···	···
				61.9	36.6	48.9	18.4	27.3	18.6	11.5	23.8	13.1	12.4	10.8

Table 4—Continued

λ (Å)	Species	E.P. (eV)	Log gf	3589	2403	2113	277	2240	1518	3011	3805	1095	2892	4437
6625.022	Fe I	1.01	−5.38	122.2	59.5	81.3	43.0	55.5	33.5	28.0	···	···	32.8	···
				110.6	54.8	85.8	38.5	50.2	43.6	34.8	38.9	29.9	42.0	23.7
6646.932	Fe I	2.61	−4.01	27.2	7.8	···	···	13.7	11.2	···	···	···	···	···
				26.3	···	16.9	7.4	13.3	19.0	6.0	···	···	10.9	···
6648.081	Fe I	1.01	−5.88	53.1	18.9	38.5	9.1	33.1	15.9	···	···	···	14.1	···
				58.6	15.7	35.0	12.6	24.8	21.3	13.3	13.8	···	15.4	···
6667.419	Fe I	2.45	−4.42	18.8	···	···	···	···	···	···	···	···	···	···
				19.0	···	20.6	7.3	···	···	···	···	···	···	···
6677.987	Fe I	2.69	−1.22	219.5	171.0	170.4	150.7	154.2	142.9	131.2	142.2	···	126.1	···
				182.3	165.1	172.5	154.0	156.8	143.8	140.7	136.1	135.2	128.2	109.3
6703.567	Fe I	2.76	−3.13	65.1	48.0	45.0	34.1	39.8	32.3	24.6	37.7	28.5	20.3	···
				68.0	51.4	60.2	29.4	46.6	37.8	30.8	38.0	33.3	31.7	24.8
6710.320	Fe I	1.49	−4.90	82.2	36.5	55.7	35.0	43.7	32.8	37.6	28.3	26.5	25.4	···
				74.7	···	57.0	30.6	45.8	33.4	···	22.4	29.1	17.9	22.0
6739.522	Fe I	1.56	−4.98	89.9	21.4	54.9	42.4	45.8	28.7	···	27.0	···	14.0	···
				62.0	···	42.5	22.0	29.3	22.2	19.8	15.9	22.6	21.1	12.4
6750.153	Fe I	2.42	−2.48	134.1	113.9	120.4	80.0	102.1	82.1	84.9	···	89.9	83.2	···
				131.6	104.6	117.3	98.7	103.3	86.3	99.5	90.2	78.8	90.8	65.9
6752.707	Fe I	4.64	−1.30	47.2	···	23.2	···	24.2	···	10.4	11.6	11.3	···	···
				45.2	···	20.2	5.4	16.8	···	11.8	9.9	···	14.7	11.2
6806.845	Fe I	2.73	−3.24	68.2	33.8	42.6	33.6	43.3	30.5	28.8	38.3	···	25.5	···
				···	···	···	···	···	···	···	···	···	···	···
6810.263	Fe I	4.61	−1.12	27.0	13.0	23.2	···	23.5	17.1	···	···	···	11.2	···
				···	···	···	···	···	···	···	···	···	···	···

Table 4—Continued

λ (Å)	Species	E.P. (eV)	Log gf	3589	2403	2113	277	2240	1518	3011	3805	1095	2892	4437
6839.831	Fe I	2.56	−3.47	65.2	30.0	47.8	···	28.5	22.3	···	···	···	···	···
				···	···	···	···	···	···	···	···	···	···	···
6586.319	Ni I	1.95	−2.95	···	···	···	···	···	···	···	···	···	···	···
				79.7	64.9	65.1	46.6	57.7	42.4	59.3	41.2	38.3	34.9	···
6643.638	Ni I	1.68	−2.01	176.4	129.8	145.3	122.4	127.6	111.0	109.7	114.5	92.9	86.6	···
				171.6	142.5	145.5	123.4	128.3	125.4	112.4	108.7	106.0	94.3	77.7
6767.784	Ni I	1.83	−1.89	137.0	121.7	113.1	107.7	102.9	89.9	87.4	88.8	97.4	89.0	···
				141.4	···	124.1	116.0	106.6	83.7	106.4	99.9	90.9	85.0	77.7
6772.321	Ni I	3.66	−1.07	31.7	31.7	29.9	23.3	28.4	21.6	17.6	16.9	26.6	15.5	···
				39.1	···	43.7	30.9	29.9	41.5	25.6	27.9	25.3	···	19.7
6774.330	La II	0.13	−1.75	35.1	17.5	24.3	···	16.1	9.3	12.0	8.1	···	···	···
				31.4	···	28.8	···	14.4	14.0	···	···	···	···	···
6645.127	Eu II	1.38	+0.42	32.1	25.2	30.4	25.2	28.6	23.4	23.7	···	14.4	···	···
				30.7	13.3	26.7	19.9	24.6	27.7	23.3	16.5	···	13.6	···

Note. — The first row of each line refers to the 1999 data, while the second row refers to the 2001 data.

Table 5. Atomic Line Parameters and Equivalent Widths for M80 Giants

λ (Å)	Species	E.P. (eV)	Log gf	1	2	3	4	5	8	11	16	23	31
6696.023	Al I	3.14	-1.35	16.1	39.5	16.2	16.3	···	72.8	38.4	38.7	7.8	55.4
6698.673	Al I	3.14	-1.65	···	17.8	···	···	···	27.6	13.5	26.3	···	27.8
6717.687	Ca I	2.71	-0.39	109.4	131.8	108.3	104.2	118.2	119.1	82.1	99.9	72.4	82.6
6599.113	Ti I	0.90	-2.06	49.6	93.0	38.1	52.6	52.6	33.1	···	···	···	···
6743.127	Ti I	0.90	-1.76	67.8	122.1	71.0	65.4	69.8	53.2	41.4	29.6	···	17.5
6606.979	Ti II	2.06	-2.85	14.4	19.8	20.7	18.3	29.3	···	···	···	···	17.2
6630.032	Cr I	1.03	-3.59	18.2	47.6	18.2	21.9	···	···	···	···	···	···
6581.210	Fe I	1.49	-4.82	63.3	83.9	55.5	50.3	62.4	59.8	46.1	46.6	16.7	33.2
6593.871	Fe I	2.43	-2.34	127.2	162.4	126.6	147.7	113.4	122.8	101.0	123.5	73.0	96.2
6608.026	Fe I	2.28	-4.02	31.6	39.6	29.1	122.6	38.2	27.4	22.2	···	···	···
6609.110	Fe I	2.56	-2.67	91.1	114.2	97.2	30.2	85.5	90.8	82.1	77.4	62.7	66.7
6609.679	Fe I	0.99	-5.87	44.4	52.2	34.5	97.0	35.3	27.3	30.9	40.0	6.8	16.7
6625.022	Fe I	1.01	-5.38	73.6	106.6	70.8	32.4	60.4	62.9	47.1	44.9	21.8	30.5
6646.932	Fe I	2.61	-4.02	15.1	17.7	12.0	68.1	12.4	···	12.6	11.1	···	···
6648.081	Fe I	1.01	-5.88	35.0	49.9	29.5	14.3	20.8	27.5	12.1	34.0	18.0	17.3
6667.419	Fe I	2.45	-4.42	14.2	24.2	12.8	24.4	10.9	···	···	···	···	4.4
6677.987	Fe I	2.69	-1.22	170.6	192.8	167.0	···	161.0	163.5	141.6	153.0	120.2	···
6703.567	Fe I	2.76	-3.13	59.4	59.4	48.3	50.1	50.9	45.5	32.1	28.9	29.2	···
6710.320	Fe I	1.49	-4.90	55.3	63.9	43.8	51.8	68.1	64.8	23.6	29.7	···	23.6
6739.522	Fe I	1.56	-4.98	40.5	36.5	33.2	35.0	22.9	···	28.5	29.8	···	14.9
6750.153	Fe I	2.42	-2.48	119.2	132.8	113.8	112.0	128.5	98.3	100.9	104.8	88.3	84.9
6752.707	Fe I	4.64	-1.30	16.3	27.0	···	11.8	···	12.6	···	13.4	···	13.0
6586.319	Ni I	1.95	-2.95	67.9	77.7	69.1	60.9	75.0	54.5	51.6	54.0	30.7	38.8
6643.638	Ni I	1.68	-2.01	147.9	173.9	142.6	139.8	157.4	122.0	114.3	133.6	98.3	97.8

Table 5—Continued

λ (Å)	Species	E.P. (eV)	Log gf	1	2	3	4	5	8	11	16	23	31
6767.784	Ni I	1.83	-1.89	127.0	171.2	116.4	128.0	138.5	119.2	103.5	123.5	87.6	92.1
6772.321	Ni I	3.66	-1.07	32.3	···	28.8	26.3	37.3	24.5	25.8	30.1	19.9	22.4
6774.330	La II	0.13	-1.75	30.5	···	26.6	23.5	15.4	31.4	20.6	17.1	···	23.3
6645.127	Eu II	1.38	+0.42	32.4	39.7	42.4	29.5	27.8	28.8	27.9	27.4	24.2	24.0

Table 6. Model Atmosphere Parameters

Star	$T_{\rm eff}$ (K)	Log g (cm s^{-2})	$v_{\rm t}$ (km s^{-1})	P/S[a]
NGC 6752				
3589[b]	4050	0.55	2.20	S
	4125	0.70	1.77	
2403	4055	0.56	2.11	P
2113	4110	0.66	2.07	P
277	4355	1.13	1.85	P
2240	4355	1.13	1.85	P
1518	4425	1.27	1.79	P
3011	4390	1.20	1.82	P
3805	4415	1.25	1.80	P
1095	4465	1.35	1.76	P
2892	4475	1.38	1.75	P
4437	4575	1.58	1.67	P
M80				
1	4045	0.60	2.12	P
2	4125	0.70	2.21	S
3	4065	0.57	2.10	P
4	4100	0.65	2.07	P
5	4175	0.79	2.01	P
8	4065	0.57	2.10	P
11	4275	0.98	1.92	P
16	4065	0.57	2.10	P
23	4490	1.20	1.74	P
31	4390	1.28	1.82	P

[a]P = preferred model from photometry; S = preferred model from spectroscopy

[b]First row refers to model parameters derived from the first-epoch spectrum, while the second row refers to model parameters derived from the second-epoch spectrum.

Table 7. Abundance Sensitivity to Model Atmosphere Variations

Abundance Ratio	$\Delta T_{\rm eff}$ ±100 K	$\Delta \log g$ ±0.2 dex	$\Delta v_{\rm t}$ ±0.2 km s^{-1}
Δ[Fe/H]	0.15	0.02	0.04
Δ[Al/Fe]	0.09	0.01	0.00
Δ[Ca/Fe]	0.13	0.01	0.10
Δ[Ti/Fe]$_{\rm I}$	0.21	0.01	0.03
Δ[Ti/Fe]$_{\rm II}$	0.03	0.09	0.02
Δ[Cr/Fe]	0.20	0.01	0.00
Δ[Ni/Fe]	0.11	0.03	0.08
Δ[La/Fe]	0.03	0.09	0.01
Δ[Eu/Fe]	0.01	0.09	0.01

Table 8. Abundances

Star	[Fe/H]	[Al/Fe]	[Ca/Fe]	[Ti/Fe]$_{\rm I}$	[Ti/Fe]$_{\rm II}$	[Cr/Fe]	[Ni/Fe]	[La/Fe]	[Eu/Fe]
NGC 6752									
3589	−1.31	+0.55	+0.33	+0.45	+0.22	−0.02	−0.15	+0.09	+0.36
2403	−1.94	< −0.20	+0.24	−0.04	+0.71	···	+0.12	+0.34	+0.62
2113	−1.60	+0.27	+0.32	+0.25	+0.64	−0.06	−0.17	+0.21	+0.57
277	−1.66	+0.42	+0.11	+0.09	+0.48	···	+0.02	···	+0.66
2240	−1.47	+0.00	+0.39	+0.28	+0.34	−0.06	−0.15	+0.08	+0.57
1518	−1.48	+0.42	+0.20	···	+0.06	···	−0.17	+0.07	+0.64
3011	−1.69	−0.25	+0.25	···	+0.23	···	0.00	+0.24	+0.76
3805	−1.57	+0.96	+0.25	+0.13	+0.54	···	−0.15	−0.10	+0.48
1095	−1.57	+0.98	+0.38	−0.05	···	···	−0.13	···	+0.45
2892	−1.55	< −0.19	+0.27	+0.16	···	···	−0.31	···	+0.41
4437	−1.58	< +0.05	+0.18	···	···	···	−0.24	···	···
M80									
1	−1.72	+0.04	+0.17	+0.09	+0.35	−0.19	−0.04	+0.44	+0.78
2	−1.47	+0.30	+0.27	+0.53	+0.22	+0.20	+0.03	···	+0.66
3	−1.82	+0.12	+0.24	+0.13	+0.57	−0.10	−0.05	+0.41	+1.05
4	−1.79	+0.11	+0.20	+0.24	+0.51	+0.03	−0.06	+0.35	+0.82
5	−1.66	−0.18	+0.41	+0.31	+0.66	···	+0.14	+0.09	+0.63
8	−1.85	+1.11	+0.38	+0.04	···	···	−0.17	+0.56	+0.84
11	−1.73	+0.54	+0.08	+0.17	···	···	−0.10	+0.35	+0.77
16	−1.94	+0.75	+0.26	−0.26	···	···	+0.02	+0.30	+0.93
23	−1.69	−0.02	+0.19	···	···	···	−0.07	···	+0.78
31	−1.66	+0.89	+0.18	−0.15	+0.46	···	−0.18	+0.54	+0.77

Table 9. Mean Cluster Abundances

Element Ratio	NGC 6752	M80
[Fe/H]	−1.58(0.16)[a]	−1.73(0.13)
[Al/Fe]	+0.51(0.36)	+0.37(0.43)
[Ca/Fe]	+0.26(0.08)	+0.24(0.10)
$[Ti/Fe]_I$	+0.16(0.17)	+0.12(0.24)
$[Ti/Fe]_{II}$	+0.40(0.23)	+0.46(0.16)
[Cr/Fe]	−0.05(0.02)	−0.02(0.17)
[Ni/Fe]	−0.12(0.12)	−0.05(0.10)
[La/Fe]	+0.13(0.14)	+0.38(0.15)
[Eu/Fe]	+0.55(0.12)	+0.80(0.12)

[a]Standard deviation